
Article:
Way, M., Luo, D., Tuley, R. et al. (1 more author) (2020) A new high entropy alloy brazing filler metal design for joining skutterudite thermoelectrics to copper. Journal of Alloys and Compounds. 157750. ISSN 0925-8388

https://doi.org/10.1016/j.jallcom.2020.157750

Journal of Alloys and Compounds xxx (xxxx) xxx

Contents lists available at ScienceDirect

Journal of Alloys and Compounds

journal homepage: http://www.elsevier.com/locate/jalcom

A new high entropy alloy brazing filler metal design for joining skutterudite thermoelectrics to copper

Matthew Way [a], Dan Luo [a], Richard Tuley [b], Russell Goodall [a, *]

[a] Department of Materials Science and Engineering, The University of Sheffield, Sheffield, UK
[b] European Thermodynamics Ltd, Wistow Road, Kibworth, Leicestershire, UK

ARTICLE INFO

Article history:
Received 14 September 2020
Received in revised form
23 October 2020
Accepted 27 October 2020
Available online xxx

Keywords:
Brazing filler metal
High entropy alloy design
Thermoelectrics
Gallium
Metal joining
Python programming

ABSTRACT

A new High Entropy Alloy (HEA) in the ZnGaCu-(AuSn) system was designed to join skutterudite thermoelectrics ($CoSb_{2.75}Sn_{0.05}Te_{0.20}$), with a diffusion barrier of Ni applied, to Cu. Such a joint could be part of a device for thermal energy recovery within automotive exhaust systems. A rapid large-scale screening calculation technique based on Python programming has been introduced to conduct the HEA selection process, resulting in a series of alloys, which have been experimentally verified. It is demonstrated that a particular ZnGaCu-(AuSn) HEA alloy can join Ni and Cu successfully; a good joint is formed, and the average electrical contact resistance of the interfaces after joining is promising at room temperature, which shows that it has the potential to improve on the existing fillers used in such applications. The alloy design methodology used here suggests a potential efficient route to design new filler metals for a wide array of applications in which existing filler metals are not suitable.

1. Introduction

Brazing is an ancient joining process with the principal advantage of being able to join dissimilar materials (dissimilar metals or metal to ceramic). In the process a brazing filler metal is used to bond the materials (known as parent materials) [1–4]. A filler metal has a lower liquidus than the parent materials and it is introduced between them and heated until it is in its molten state; on solidification, a permanent and strong metallic bond is formed. *Brazing* fillers are those with a liquidus above 450 °C, and *soldering* fillers have a liquidus below 450 °C, although this temperature is an arbitrary separation and the two processes are inherently similar.

Brazing filler metal development is an enabling technology in many engineering fields ranging from nuclear fusion to nanoelectronics [5–8]. One specific area where development of fillers is needed is in the joining of thermoelectric components [8]. Thermoelectric generators (TEGs) have been applied in many areas and are considered to have the potential to improve efficiency in many areas [9–12], such as in automotive exhausts [12]. TEGs have unique advantages over other technologies, being simple and reliable and having no moving parts, as well as being small in size and flexible [13]. One of the most promising medium to high temperature TEG materials, CoSb3-based n-type skutterudite thermoelectrics, could have an excellent thermoelectric figure of merit (ZT > 1.3 between 300 °C and 600 °C) and are viewed as a more applicable and environmentally friendly thermoelectric material than some alternatives (e.g. PbTe [14]). However, to achieve the best performance and power production in $CoSb_3$-based thermoelectrics requires operating at an optimum temperature of 550 °C [12,15]. At the same time, sublimation of Sb increases greatly above 620 °C [16]. Thus, the optimal melting temperature range for a filler metal to braze such thermoelectrics would be 550–620 °C (melting below this optimal range may lead to remelting at service temperatures, and melting above this range may lead to thermal degradation of the thermoelectric components during the brazing cycle due to loss of Sb).

There exists a wide range of commercially available filler metals, adapted to fit a broad array of general applications which could be chosen for use in this application according to the melting range. Many of these brazing and soldering filler metals can be found in ISO standards [17,18]. They are organised into 'families' which largely denote the principal element in that group of filler metals [17,18]. Whilst many other solders and brazing filler metals do exist, they are often specifically developed for niche applications.

However, very few brazing filler metals exist in the melting

* Corresponding author.
E-mail address: r.goodall@sheffield.ac.uk (R. Goodall).

https://doi.org/10.1016/j.jallcom.2020.157750

Table 1
The solid solution filtering parameters used to attempt to find suitable filler metal compositions.

Parameter	Accepted values
Atomic Size difference (δ)	$0 < \delta < 5$
Enthalpy of mixing (ΔH_{mix})	$-2.5455\delta - 2.4545 < \Delta H_{mix} < -\frac{15}{11}\delta + \frac{70}{11}$
Entropy of mixing (ΔS_{mix})	$11 < \Delta S_{mix} < \infty$
Rule of mixtures melting temperature (T_m)	$550°C < T_m < 620°C$

range of interest for the application in this study from the solidus and liquidus temperature ranges in both solder and braze ISO standards [17,18]. In fact, only 2 silver based filler metals and 10 aluminium based fillers are within the optimal temperature range. Due to both silver based fillers containing the restricted element cadmium [19] they are undesirable for this application. Additionally, silver-antimony compounds (hexagonal close packed $P6_3/mmc$ zeta (ζ) phase and/or the tetragonal P4/mmm epsilon (ε) phase) could form due to the excessive diffusion of Ag into the skutterudite materials after passing through the Ni diffusion barrier during the brazing process [20], which is detrimental to the skutterudite materials performance. In addition, copper (a common electrode material for thermoelectric devices [21]) readily forms an array of high hardness intermetallic compounds with aluminium (including Cu_2Al, Cu_3Al_2, CuAl) [22], restricting the use of aluminium based fillers. As such, it can be concluded that no current commercially available filler metal is suitable for the application in question (although sometimes, in the absence of better alternatives, filler metal meeting the compositional requirements for ISO 17672 Ag-155 [17], a general purpose filler metal, is used), providing the impetus to develop a new alloy.

New materials as filler metals have attracted more and more attention, including that paid to bulk metallic glasses [23] and metal foams [24], but only recently has research begun to investigate the potential for High Entropy Alloys (HEAs; also know by other names, such as Complex Concentrated Alloys, CCAs, particularly when they are multiphase) to be used as filler metals [25–27]. HEAs are multi-principal component alloys with high mixing entropy, containing five or more elements without any of them dominating the composition [28–30]. They often show unique properties (which have been suggested to arise from interactions inherent to the alloys [31]), some of which could be of use for filler metals. For example, a random solid solution (RSS) could be promoted in HEAs due to the high entropy contribution to mixing [31], allowing brittle phases to be avoided when adding large amounts of elements to control melting point, wetting or flow behaviour over a very wide temperature range. It may also permit elements normally incompatible with the parent materials to be added to the filler metals to improve specific properties of the joint. Moreover, the multicomponent nature of HEAs could mediate the transition in a joint between dissimilar materials.

It has been demonstrated that a Ni–Mn–Fe–Co–Cu HEA is able to join Inconel® 718 with good mechanical properties at brazing temperatures up to 180 °C above the liquidus [32]. Tillman et al. [33] used Ge and Sn dopants in a CoCrCuFeNi alloy to lower its melting range to temperatures similar to filler metal MBF 50A, with the germanium doped CoCrCuFeNi filler forming joints with 42.2% of the strength of similar joints formed with MBF 50A. Hardwick et al. [34] also designed a novel NiCrFeGeB HEA which successfully joined Inconel® 718 with a 1100 °C braze temperature and a hold time of 15 min. Wang et al. [35] brazed SiC ceramics using a CoFeCrNiCu HEA filler, in which $Cr_{23}C_6$ phase formed due to reaction at the interface and a high shear strength was found benefitting from the formation of solid solution in the brazing seam. However, compared to the range of joining situations in which they could be applied, research on HEAs as filler metals is highly limited [25–27,32–36]. The difficulty of developing HEA filler metals is increased by the wide palette of elements that could be considered (the ISO standards for brazing filler metal compositions alone include specifications for 29 different elements), and a more comprehensive search strategy is needed. Therefore, in this study, we have developed a rapid large-scale Python programming screening technique to aid with development. We have used the approach to develop a new HEA filler metal for joining of skutterudite thermoelectric components (brazing Ni-coated skutterudite materials to Cu) in automotive exhausts, as a demonstration of the potential of this approach to be applied to filler metal development in many fields.

2. Alloy development strategy

Much research has been undertaken into the development of HEA formation parameters to find methods to rapidly screen potential HEA compositions for those likely to form single phase solid solution alloys. To make the screening process as efficient as possible, and thus allow screening of the widest range of potential compositions, we have used 3 parameters from work which assesses the likelihood of solid solutions being formed when theoretical mixes of elements were made: the atomic size difference, the enthalpy of mixing and the entropy of mixing [37] given by Equations (1)–(3) below.

1) Atomic Size Difference (δ)

$$\delta = 100\sqrt{\sum_{c_i}^{n} C_i\left(1 - \frac{r_i}{\overline{r}}\right)^2} \tag{1}$$

where c_i is the atomic percentage of element i and r_i is its atomic radius. $\overline{r} = \sum_{i=1}^{n} c_i r_i$.

2) Enthalpy of Mixing (ΔH_{mix})

$$\Delta H_{mix} = \sum_{i=1,\ i\neq j}^{n} \Omega_{ij} c_i c_j \tag{2}$$

in which Ω_{ij} = 4*(mixing enthalpy of binary liquid alloys).

3) Entropy of Mixing (ΔS_{mix})

$$\Delta S_{mix} = -R\sum_{i=1}^{n} c_i \, lnc_i \tag{3}$$

Zhang et al. [37] plotted the atomic size difference of various HEA systems against their enthalpy of mixing to demonstrate that particular parameter values appear to indicate an increased likelihood of solid solution formation. An apparent region of greatest probability for solid solution formation was identified, with approximate boundaries given by the formulae for the atomix size

Table 2
The successful systems with compositions which passed the filtering parameters (the number of compositions passing in each system is indicated) and the specific composition within each system with the lowest atomic size difference, which was selected for manufacture (Total:100.00).

System	No. passing compositions	at%									
		Al	Ni	Cu	Zn	Ga	Ge	In	Sn	Au	Bi
ZnGaCu-(Al)	3916	34	–	17	33	16	–	–	–	–	–
ZnGaCu-(Ni)	36	–	12	25	34	29	–	–	–	–	–
ZnGaCu-(NiGe)	62	–	6	28	32	32	2	–	–	–	–
ZnGaCu-(AuSn)	4	–	–	30	36	26	–	–	2	6	–
ZnGaCu- (AuBi)	1	–	–	30	36	26	–	–	–	6	2

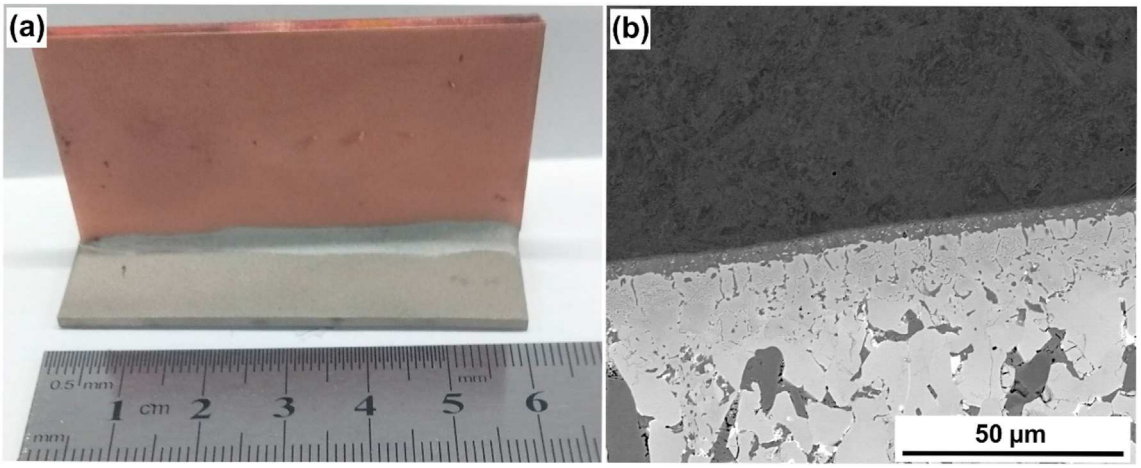

Fig. 1. Image of a joint brazed with ZnGaCu-(AuSn) alloy: (a) micro image and (b) SEM image showing the filer metal interface.

Table 3
The determined, nominal compositions and impurity of alloy ZnGaCu-(AuSn).

Composition	Elements (wt%)								Total (wt%)
	Cu	Zn	Ga	Sn	Au	C	N	O	
Nominal	25.45	31.42	24.20	3.17	15.77	–	–	–	100.00
Determined	26.19	31.19	24.25	3.07	15.65				100.35
Impurity	–	–	–	–	–	0.007	0.001	0.024	–

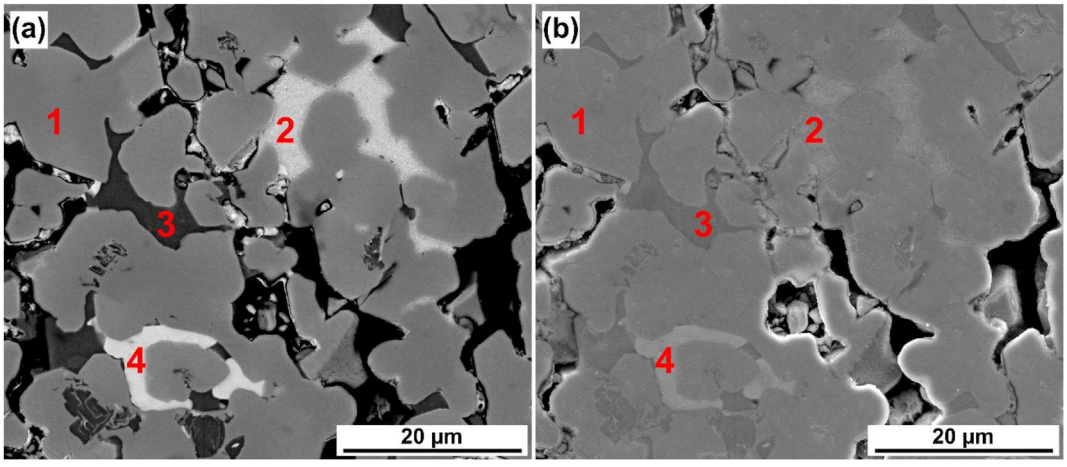

Fig. 2. SEM images of ZnGaCu-(AuSn) alloy: (a) BSE and (b) SE microstructure.

difference and $-2.5455\delta - 2.4545 < \Delta H_{mix} < -\frac{15}{11}\delta + \frac{70}{11}$ for the enthalpy of mixing in Table 1 [37].

A script written using the Python programming language (Enthought canopy software) was used to select elements and compositions, and perform the required parameter calculations. Two arrays have to be generated before the calculations can proceed. The first array controls the elements to be selected from, having a column for each element and a row for each system that is

Table 4
Composition of phases identified with EDX spot mapping in ZnGaCu-(AuSn).

Phase number	Composition (wt%)						
	Cu	Zn	Ga	Sn	Au	O	Si
1) Primary solid solution	32.4	36.8	10.6	0.1	19.4	0.6	–
2) Predominantly tin phase	2.0	2.4	3.9	83.9	2.9	4.4	0.5
3) $CuGa_2$	30.3	2.5	65.5	0.1	0.9	0.6	0.1
4) Gold-gallium phase	5.0	6.4	36.4	0.5	49.3	1.4	0.2

to be assessed. The second type of array controls the compositions and is calculated separately, using a step size of 1 at% [27]. Following the calculation, the empirical parameters above and a rule of mixtures estimate for the melting temperature (equation (4) [27]) are used to filter large numbers of potential alloy systems, applying the limits in Table 1.

$$T_m = \sum_{i=1}^{n} c_i (T_m)_i$$

where c_i and $(T_m)_i$ are the atomic percentage and the melting temperature of element i, respectively [27]. It should be noted that this is an initial estimate of melting temperature only, suitable as an initial filter for the material selection process, as it is not capable of indicating the presence or effect on T_m of the formation of eutectics or high temperature phases for example.

3. Experimental materials and procedures

3.1. Materials preparation

The production of alloys was carried out using a 2.2 kW Ambrell induction melter in 20 g batches. The raw elements used as

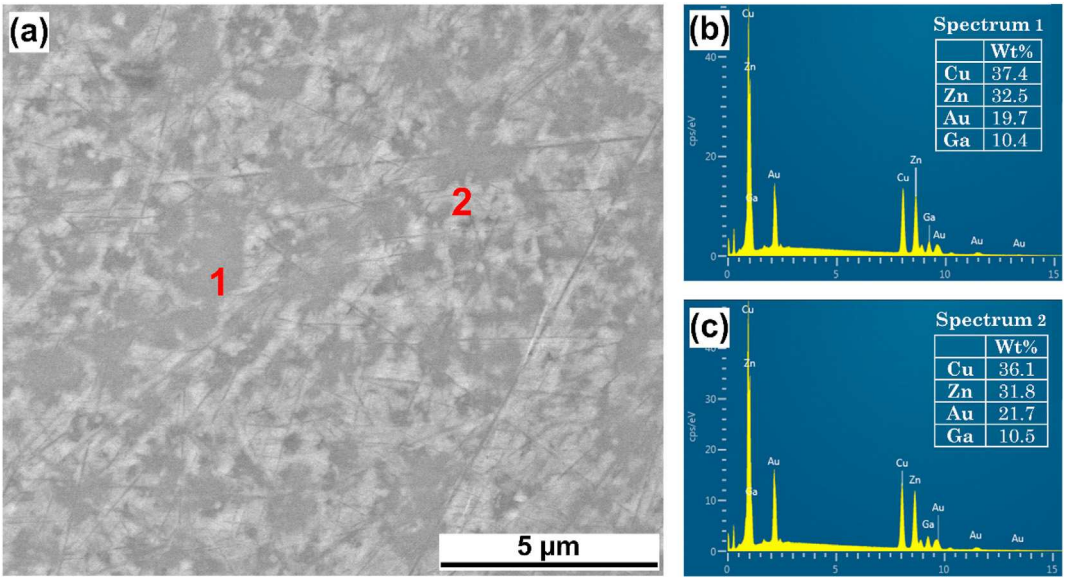

Fig. 3. (a) BSE image of alloy SS-Au-1, (b) EDX spectra of area 1 in (a) and (c) EDX spectra of area 2 in (a).

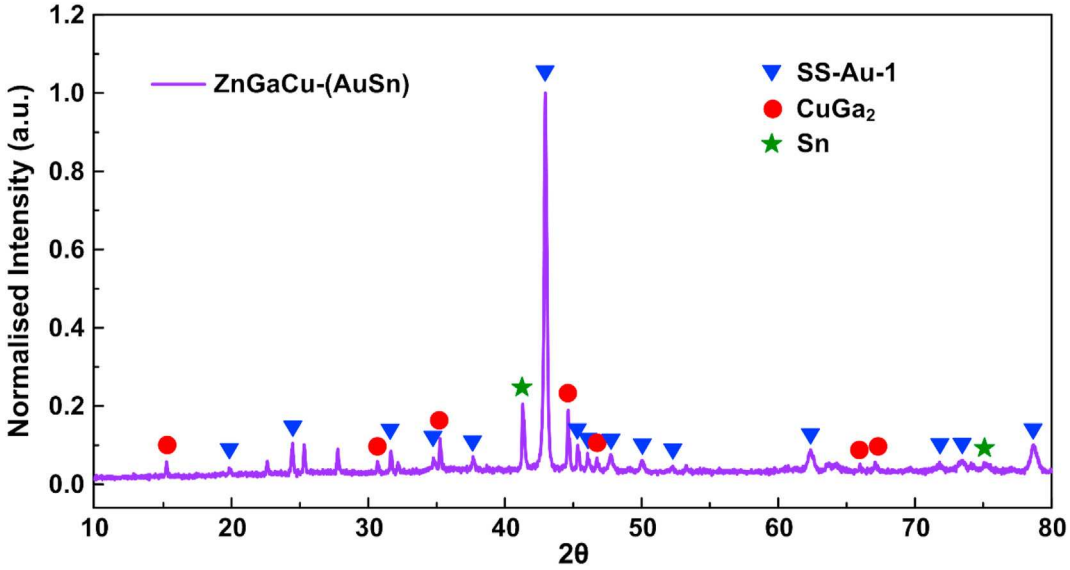

Fig. 4. XRD diffraction pattern for ZnGaCu-(AuSn) alloy. Peaks are matched to the solid solution alloy SS-Au-1, $CuGa_2$ (PDF card number: 00-025-0275) and elemental tin (PDF card number: 01-083-8001).

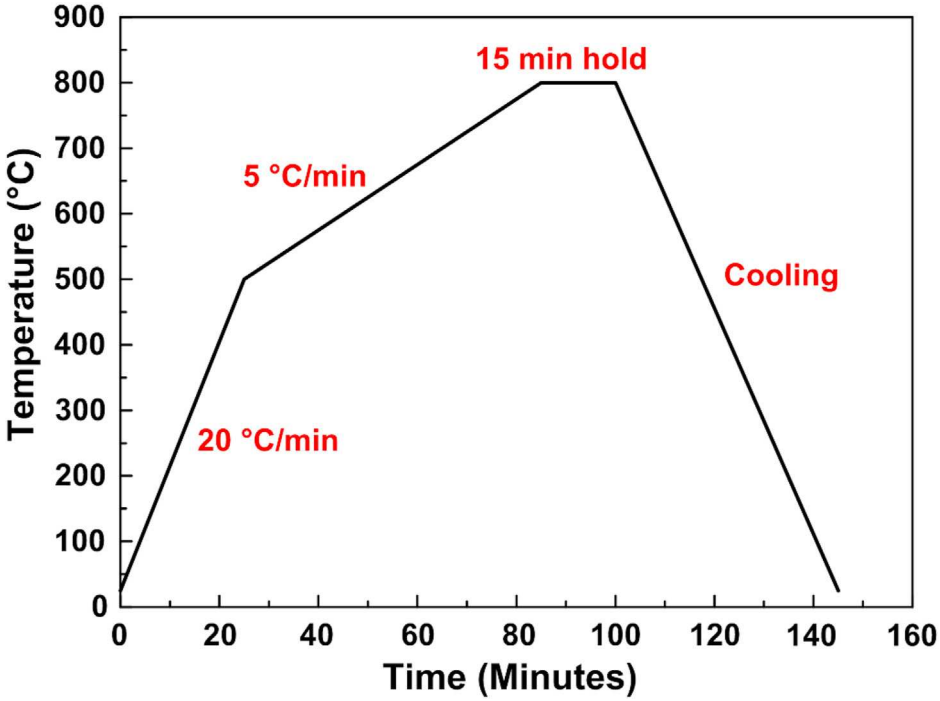

Fig. 5. Heating schedule used in wetting experiments of ZnGaCu-(AuSn) alloy.

constituents of each alloy were all >99.99% pure and weighed using a Precisa XB 120A balance to an accuracy of 0.01 g before being transferred to a Plumbago (graphite-clay) crucible which had been pre-baked at 1000 °C to remove any surface coatings and/or moisture. The alloy constituents were covered with a layer of borax (sodium tetraborate anhydrous 99.5% ($B_4Na_2O_7$), Sigma-Aldrich, UK) which melted during the production process and protected the alloy from oxidation during melting and casting. Casting of the alloy was into a cylindrical copper mould. Standard ISO 17672 Ag-155 [17] filler, with composition Ag(54/56)Cu(20/22)Zn(20/24)Sn(1.5/2.5) (minimum/maximum tolerances in wt%) (Johnson Matthey, UK) was used for comparison. Skutterudite materials were obtained from Johnson Matthey (UK), and were coated with a 0.7 μm layer of Ni by thermal deposition, using a Wordentec EVAP300 thermal evaporator with a deposition rate of 1.6Ås^{-1}. The growth pressure in the chamber was 2.1×10^{-6} mbar and the nickel powder used had a purity of 99.5% with a maximum particle size of 250 μm.

3.2. Brazing trials

Once selected and manufactured, samples of each of the alloys were subjected to simple preliminary brazing tests to assess the 'brazeability' of each alloy. A standardised T-shaped butt joint was formed between a coupon of O.F.H.C. copper (dimensions 60 mm × 30 mm × 3 mm; 99% pure, Goodfellow Cambridge Ltd, UK) and a similar coupon of annealed nickel (99.4% pure, Goodfellow Cambridge Ltd, UK). The best performing alloy system was taken forward for further examination.

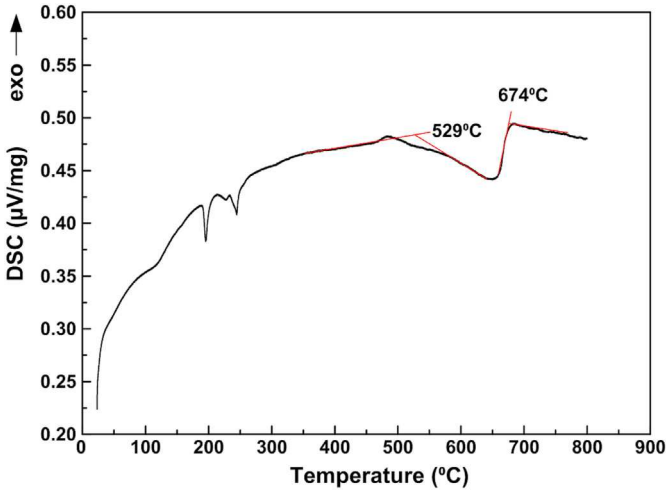

Fig. 6. DSC for ZnGaCu-(AuSn).

3.3. Characterisation

Compositions of alloys were verified using Inductively Coupled Plasma-Optical Emission Spectroscopy (ICP-OES) performed to ISO 17025 on a Thermo ICAP instrument (6500). Additionally, impurity levels of nitrogen and oxygen were assessed using LECO elemental analysis, measured using inert gas fusion with a helium carrier gas. Nitrogen content was measured using thermal conductivity and the

Table 5
Initial and average final contact angles for filler metals Ag-155 and ZnGaCu-(AuSn).

Alloy	Initial contact angle (°)	Average final contact angle (°)	Standard error of averaged final contact angle ($S_{\bar{x}}$)
Ag-155	129.6	24.2	±0.8
ZnGaCu-(AuSn)	147.3	47.0	±1.8

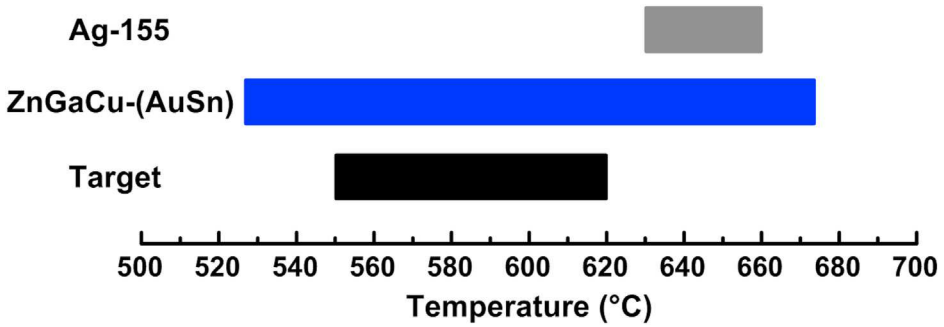

Fig. 7. Melting range for ZnGaCu-(AuSn) compared to the target range and the melting range for Ag-155 listed in ISO: 17,672 [17].

oxygen content with infrared. Carbon levels were detected using infra-red detectors as the sample was burnt under flux in an oxygen atmosphere.

An Inspect F50 Scanning Electron Microscope (SEM) equipped with a Field Emission Gun (FEG) using both Secondary Electron (SE) and Back Scattered Electron (BSE) imaging with Energy Dispersive X-ray spectroscopy (EDX) was used. The accelerating voltage was 20 kV for imaging with a spot size of 4.0.

XRD diffraction patterns were obtained using a Bruker D2 phaser with Cu Kα radiation and a 0.6 mm divergence slit. The sample was scanned over the incident angle range of 10–80º. The diffraction pattern was then compared to diffraction patterns in the PDF-4+ database using the Sieve + software from the International Centre for Diffraction Data (ICDD).

The melting temperature range was determined by Differential Scanning Calorimetry DSC using Netzsch STA 449 F3 Jupiter. Samples were tested in alumina crucibles with alumina lids over the temperature range of 25 °C –800 °C. Both sample and reference were heated at a rate of 10 °C min^{-1} under a protective atmosphere of nitrogen (N_2) at a flow rate of 50 ml min^{-1}.

3.4. Wetting test

A modified sessile drop wetting test experiment was performed on copper substrates. The copper substrates (20 mm × 20 mm × 2 mm in dimensions, O.F.H.C purity) were used. The samples were then loaded into a Thermal Technology LLC model 1160-2560-12 furnace which was filled with an atmosphere comprising of 90% Ar and 10% H2. An ImagingSource DMK 23GP031 camera was set up to take side-on images at 1 s intervals of the filler metal and substrate within the furnace. The temperature of the furnace was then raised according to the heating schedule depicted in Fig. 5 from room temperature to 800 °C at 20 °C per minute from room temperature to 500 °C and then 5 °C per minute from 500 °C until 800 °C. Once 800 °C was reached the sample was held at a steady temperature for 15 min before being furnace cooled to room temperature at a rate of approximately 20 °C per minute. This heating profile was much more gradual than would be experienced during actual brazing, where the entire process only takes a few minutes. This slower rate was used in order to allow the molten droplet to approach the equilibrium contact angle during the measurement, but it should be noted that the difference in rate could mean that different wetting behaviour may be encountered in a brazing situation. During the heating cycle from 500 °C onwards photographs were taken by the camera of the sample at 1 s intervals and these images were analysed by the software "Drop_angle" (Developed at the Berkeley National Lab in November 2002 by Laurent Gremilard with the help of Nicole Rauch and Eduardo Saiz–version 7.5.45 [38]) to extract contact angle information.

3.5. Contact resistance test

While the thermoelectric ZT value is very important in gauging the capability, the contact resistance is the main parameter of the joint which will affect the overall performance, and so this is explored here. Electrical contact resistance at the interfaces in a brazed assembly were measured at room temperature. Using equipment and a test configuration developed for testing interfaces in thermoelectric materials [39], 2 pieces of n-type skutterudite thermoelectric ($CoSb_{2.75}Sn_{0.05}Te_{0.20}$, the ZT of which varies with temperature, having a maximum ZT of 1.13 at around 405 °C [40]) of 2.5 mm × 2.5 mm × 3 mm were brazed with a copper interlayer using the alloy developed in this study to produce a sample as shown in Fig. 8. The contact resistance was measured using a Keithley 2400 (with resistance measured by a linear fit to bidirectional pulses across a range of currents) laterally across the interfaces present using a 4 probe–setup [39]. The positioning of the probes had a geometric resolution of ~50 μm, by automated stage and microprobe set up (based on a DPP205 probe positioner from Cascade Microtech, Inc.).

4. Results

4.1. Python calculations

Investigations into suitable high entropy materials for use as brazing filler metals required the narrowing of the elements to a pool of potentially suitable candidate elements. This was undertaken by eliminating elements which were gaseous or liquid at room temperature and those which were radioactive, too toxic or too reactive to be safely handled and processed. Following this filtering, the remaining 19 elements under consideration were Al, Si, V, Cr, Mn, Fe, Co, Ni, Cu, Zn, Ga, Ge, Ag, In, Sn, Sb, Te, Au and Bi. However, these elements also must meet the thermoelectric application requirements: (a) Melting temperature: The alloy must have a suitable melting temperature (therefore extensive amounts of elements with high melting temperatures are unlikely to be acceptable, barring the presence of substantial eutectics; As such, elements whose melting temperature was <120% of the maximum of optimal temperature range (T_{opt} = 550–620 °C), e. g T_m < 744 °C, were preferred. However, elements with slightly higher melting temperature than this could also be considered (e.g. Ge). Ni and Cu are kept for compatibility with parent materials and Au could improve the wetting. (b) Diffusion coefficient: Filler metal elements should not diffuse through the nickel diffusion barrier; elements whose diffusion coefficient being the same order of magnitude (or a lower) compared to the self-diffusion coefficient of nickel (2.46×10^{-19} cm^2s^{-1}) at 773 K were preferred [41–44] (although others could be included if there were compelling advantages with respect to other selection criteria, e.g. Al, In and Sn are chosen for lowing the melting temperature). (c) Antimony compounds:

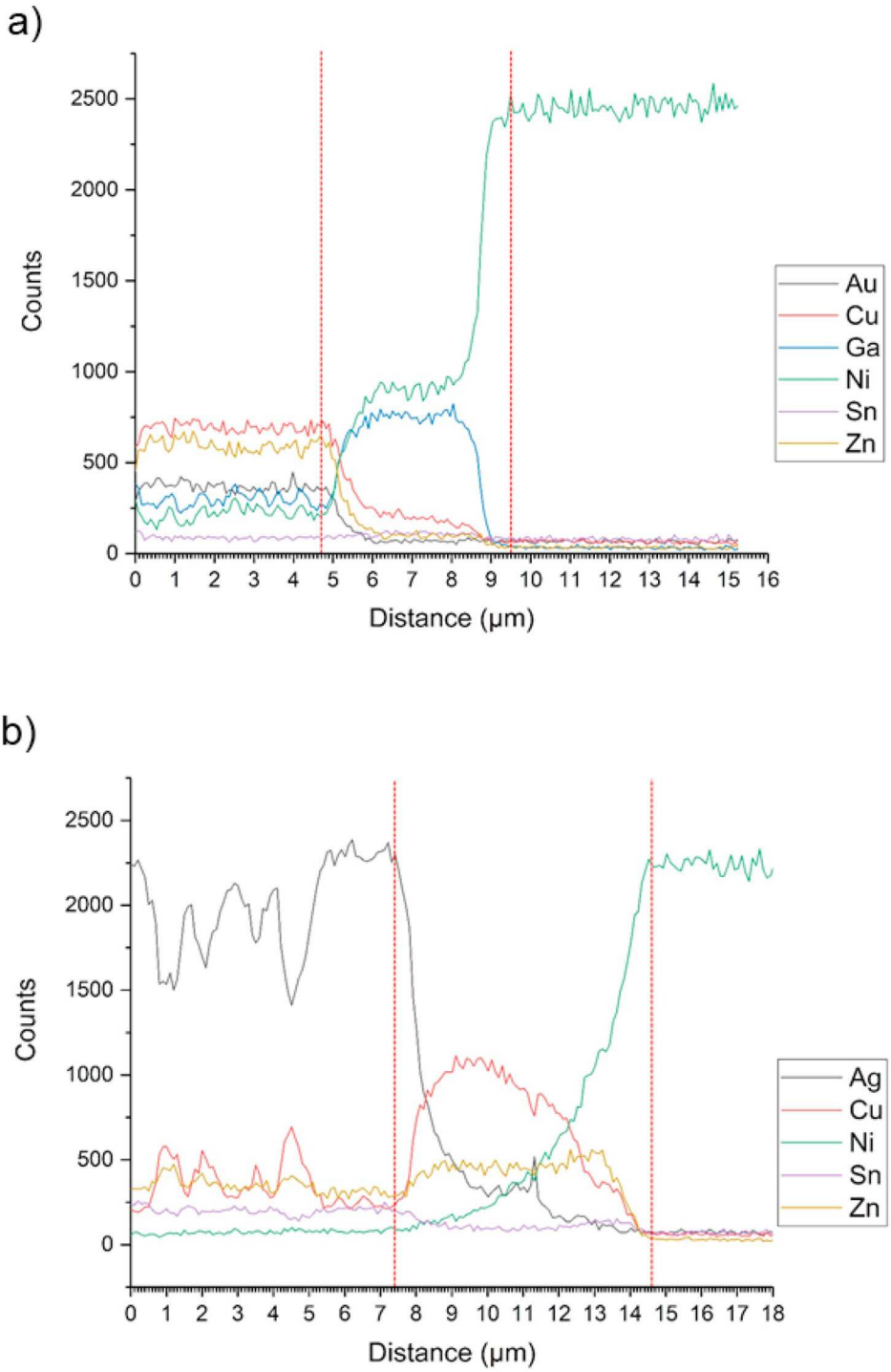

Fig. 8. Examples of Energy Dispersive X-Ray Spectrometry (EDX) line scans showing the variation in the intensity of the signal from each element present, across the joint between a) ZnGaCu-(AuSn) and b) ISO: 17,672 Ag-155 and nickel. The boundaries of the region identified as the diffusion zone from the compositional variation are indicated with red dotted lines. (For interpretation of the references to colour in this figure legend, the reader is referred to the Web version of this article.)

Formation of detrimental antimony compounds in the thermoelectric are to be avoided, but Zn, Ga and Bi are kept for lowing melting temperature. Therefore, after removing those elements which do not meet the three key requirements above, the list was reduced to 10 suitable elements (Al, Cu, Zn, Ga, Ni, Ge, Sn, In, Au and Bi), and these were used for the Python program. As described in the alloy design section, this program takes all possible combinations of 5 elements from the 10 provided, and calculates the parameters described by Equations (1)–(4) (the atomic size difference, the enthalpy of mixing, the entropy of mixing and the rule of mixtures melting point) for every possible composition, in the range of 5–35 at% of each element, in 1 at% increments. After these calculations create a database of parameters for all the possible compositions in the range, this is filtered using the criteria in Table 1 to estimate the formation of HEAs. This found that the 5 alloy systems in Table 2 were potentially suitable, having at least

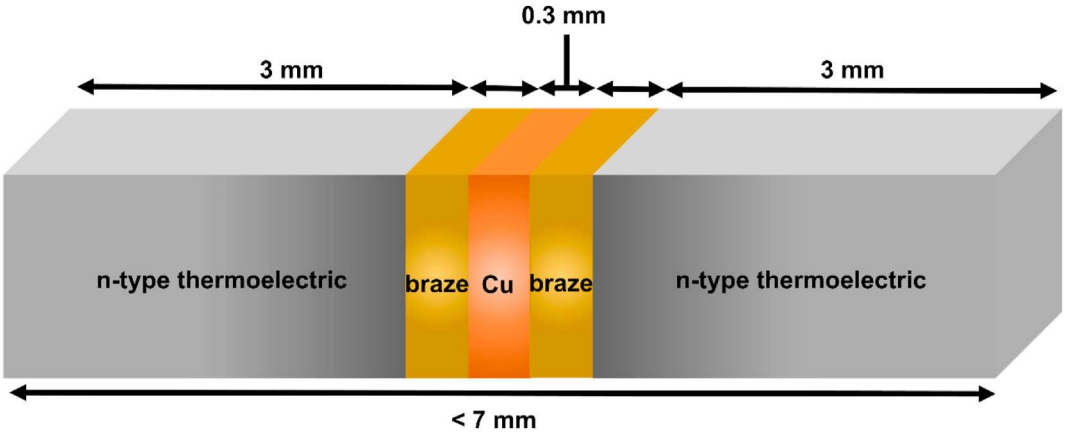

Fig. 9. Diagram of the brazed thermoelectric sample used to assess the contact resistance of the filler metal-thermoelectric interface.

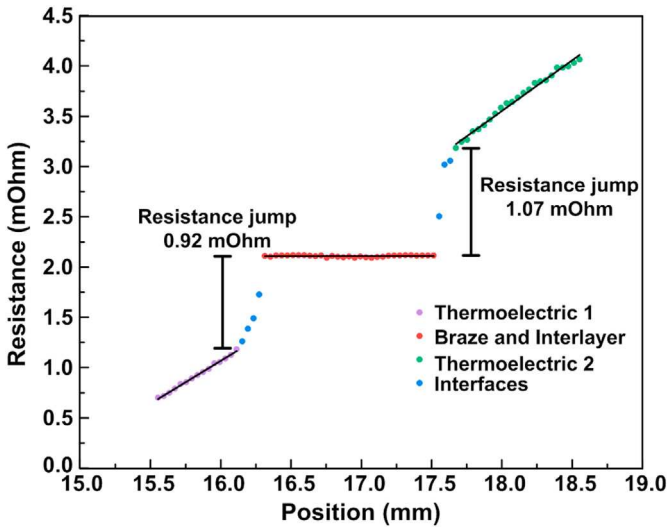

Fig. 10. Graph of resistance against lateral position along the brazed thermoelectric sample. The jumps in resistance correspond to the interface between filler metal and thermoelectric.

one composition that passed the limits. Where multiple compositions within a single system passed the applied selection filters (which was often the case; for example 3916 different compositions for ZnGaCu-Al system were found suitable, Table 2) the alloy composition with the lowest atomic size difference in each system was selected as the composition to be taken forward. The specific composition selected in each alloy system is recorded in Table 2, which also gives the nomenclature used to refer to these alloys in the rest of this work, and these alloys were experimentally produced for further investigation.

4.2. Brazing testing

To assess the brazeability of each alloy, the five alloys were subjected to simple preliminary brazing tests. A standardised T-shape butt joint was formed between a coupon of copper and a similar coupon of annealed nickel. As compared with the rest of alloys, alloy ZnGaCu-(AuSn) presented the best brazing performance. A macro image of the brazed joint formed using this alloy, and an SEM image of the interface between filler metal and copper coupon can be seen in Fig. 1(a) and (b), respectively. As alloy ZnGaCu-(AuSn) can apparently successfully bond the necessary parent materials it was chosen for further investigation.

4.3. Filler metal

Table 3 shows the determined and nominal compositions of ZnGaCu-(AuSn); it can be seen that the composition is as intended and determined constituent weights are within ±0.8 wt% for all constituents. Additionally, impurity levels were assessed to determine contamination levels and verify the effectiveness of the borax glass at preventing oxidation of the melt pool during processing. Carbon, nitrogen and oxygen levels are also shown in Table 3. All measured impurities levels were below 0.025 wt%.

Fig. 2 shows BSE and SE micrographs of ZnGaCu-(AuSn). It shows a multiphase character, and therefore could be termed a CCA, rather than a HEA by those definitions which require a single phase structure. All 4 phases identified in the SEM images were EDX spot mapped in 3 separate locations and the average composition of each phase found. These average compositions are recorded in Table 4. Additionally, an XRD diffraction pattern was obtained of ZnGaCu-(AuSn) to independently confirm the phases. The $CuGa_2$ tetragonal phase and elemental tin were found. However, many peaks in the pattern could not be suitably matched and were thus suspected to belong to the primary solid solution phase identified from EDX, which did not appear to have a PDF card entry in the database, and dis not correspond to the patterns of a simple structure. In order to assess if this was the case, a new alloy, designated SS-Au-1, was manufactured with the composition of the primary solid solution determined from the EDX point scans in Table 4. Fig. 3 shows the BSD microstructure with EDX results at two different positions in the SS-Au-1 alloy. It can been see that SS-

Table 6
The measured contact resistances of both interfaces in the thermoelectric sample brazed with ZnGaCu-(AuSn).

Sample	Surface area of interface (cm^2)	Resistance discontinuity (mΩ)		Electrical contact resistance ($\times 10^{-5}$ Ωcm^{-2})		
		Interface 1	Interface 2	Interface 1	Interface 2	Average
1	0.112	0.92	1.07	10.4	12.0	11.2

Au-1 was a largely single phase structure with the variations between areas shown in the BSE images being very small in Fig. 3(b) and (c). The diffraction pattern for this sample was then used to match to peaks on the original ZnGaCu-(AuSn) sample pattern, to more clearly attribute peaks to the primary solid solution phase. The ZnGaCu-(AuSn) diffraction pattern with the peaks matching the SS-Au-1 alloy, as well as the $CuGa_2$ and tin PDF cards are labelled in Fig. 4.

4.4. Wetting testing

Wetting assessment of ZnGaCu-(AuSn) in this study was made in comparison to Ag-155 filler metal as a benchmark. An initial contact angle was recorded upon the alloy first melting, and an average final contact was calculated once the alloy settled at its final contact angle. The initial contact angles of Ag-155 and ZnGaCu-(AuSn) are 129.6º and are 147.3º, respectively; these are high and seem to indicate poor wetting, but that the early stages the alloys may not be fully molten and equilibrium will not have been established. The average final contact angles, which are more indicative of the wetting behaviour, are 24.2º and 47.0º, respectively. The initial and final contact angles of both ZnGaCu-(AuSn) and Ag-155 are shown in Table 5.

4.5. Melting temperature

Fig. 6 shows the DSC curve of the ZnGaCu-(AuSn) alloy, indicating that the melting range of this alloy is 529–674 °C. Fig. 7 shows the ideal melting temperature (the target) for this application, in comparison to the standard values for Ag-155 and those measured for ZnGaCu-(AuSn). The target melting range, and that of Ag-155 are 550–620 and 630–660 °C [17], respectively.

4.6. Diffusion investigation

In order to assess the diffusion distance of filler metal constituents of Ag-155 and the ZnGaCu-(AuSn) alloy in nickel, EDX line scans were taken across the interface between nickel and filler metal on nickel plate brazed joints formed with each filler metal. 10 line scans were taken in 3 different locations on each sample and the width of the diffusion zone measured. Examples of these traces in ZnGaCu-(AuSn) and a reference joint with Ag155 are shown in Fig. 8(a) and b respectively. The average diffusion distance zones for Ag-155 and ZnGaCu-(AuSn) are 7.0 μm and 4.8 μm, respectively. Therefore, the diffusion distance of the constituents of the new filler metal ZnGaCu-(AuSn) is <70% that of the Ag-155 filler metal.

4.7. Contact resistance

Fig. 9 shows a schematic of the sample used in the contact resistance assessment of skutterudite thermoelectric material ($CoSb_{2.75}Sn_{0.05}Te_{0.20}$), ZnGaCu-(AuSn) and copper. A graph of resistance against lateral position along the sample was produced by the motion of the mobile probe along the sample and can be seen in Fig. 10. Substantial resistance jumps can be seen at approximate axis positions of 16.25 mm and 17.5 mm measuring 0.92 mΩ and 1.07 mΩ in magnitude which correspond to the interface between filler metal and thermoelectric. The linear section in the centre of the resistance plot indicates that the resistance of the interface between filler metal and copper interlayer is negligible.

5. Discussion

Design of new HEAs presents a substantial challenge. In the periodic table, there are 38 common elements that feature in some of the alloys in current use: Li, C, N, O, Mg, Al, Si, Ti, V, Cr, Mn, Fe, Co, Ni, Cu, Zn, Ga, Ge, Sr, Y, Zr, Nb, Mo, Ru, Rh, Pd, Ag, In, Sn, Sb, Hf, Ta, W, Ir, Pt, Au, Pb and Bi. Choosing any five from this list will give more than half million systems that could be explored. Even if the search can be narrowed because of the characteristics (desirable or undesirable) of particular elements, the amounts can be varied:

$$\boldsymbol{N} = \frac{(\boldsymbol{P} + \boldsymbol{C} - 1)!}{(\boldsymbol{P}!)(\boldsymbol{C} - 1)!} \tag{4}$$

N, C and P is the number of permutations, elements and parts (100/interval), respectively; for example, there are 4,598,126 different possible alloy compositions for 5 fixed elements allowed to vary in 1 at% increments. A pure combinatorial approach will not be effective, and it is important to find an efficient way to design alloy systems; in this some help can be obtained from specific applications which introduce different criteria which can be selected for. Python programming can provide a large-scale method to select the elements and compositions, and to calculate certain parameters for assessment and ranking. After the calculation by using Python code based on rules from Zhang in Table 1 [0.37], five alloy compositions were chosen, Table 2. Finally ZnGaCu-(AuSn) was selected due to showing the best brazing performance as compared with the other four alloys; Ni and Cu were joined using the ZnGaCu-(AuSn) as the filler metal, Fig. 1(a). The SEM image shows the good joining (characterised by absence of cracks and porosity, and uniform structure without large brittle phases apparent) at the micro scale in Fig. 1(b). While we have here focussed on the interaction between the filler and nickel, as the thermoelectric material is refined and selected, it would be important to investigate the stability of the nickel barrier layer on a junction between thermoelectric and copper, and any possible interactions between filler and thermoelectric that may result. The analysis also shows that the measured composition of ZnGaCu-(AuSn) is close to that designed, with acceptable levels of carbon, nitrogen and oxygen, Table 3.

Fig. 2 shows that multiple phases exist in ZnGaCu-(AuSn), including the solid solution (which was remade as alloy SS-Au-1) Sn, $CuGa_2$ and Au–Ga phases. Solid solutions are more likely to form for the values of the parameters selected for this alloy, but the discrimination is not perfect and it has been observed that intermetallics may also form under these conditions [27,37].

The wetting ability of filler metals on parent materials is in most cases essential for brazing. In the well-known Young's equation, the contact angle θ between the solid and liquid is used to define the wettability, with wetting occurring $\theta < 90^\circ$ but not when $\theta > 90^\circ$ [8]. As can be seen from the values in Table 5, both Ag-155 and ZnGaCu-(AuSn) initially (at the first formation of a droplet shape) showed angles that would suggest non-wetting, 129.6° and 147.3° respectively. As the temperature was raised, over the temperature range 750 °C–800 °C (the maximum temperature used in the test) the contact angle of ZnGaCu-(AuSn) appeared to stabilise (within a standard error of ±1.8°) at an angle of 47.0° (the equivalent value for Ag 155 was 24.2°), indicating that it wetted the parent material suitably.

As compared with Ag-155, the melting range of ZnGaCu-(AuSn) (529–674C, Fig. 6) is wider, but, unlike Ag-155, it contains the target range (550–620 °C, Fig. 7). It is quite common for filler metals to be used at temperatures below their liquidus (for example, in the brazing of aluminium, where there is a limited margin between the melting point of the filler and the parent materials), and this should be possible as long as the liquid fraction is sufficiently large to permit flow. As ZnGaCu-(AuSn) has been designed using a quick screening method, it is also likely that the melting range could be optimised by compositional adjustment in

further study.

Diffusion plays an important role in the brazing process, and in the performance relevant to this application. While some inter-diffusion is common in brazed joints, and usually is necessary, excessive diffusion is often detrimental to the performance [32]. Inter-diffusion between filler metal and parent material can cause a change of composition, which could influence the brazing process, or the mechanical properties of the joint. In this specific application, the thermoelectric can be degraded by reaction with elements from the filler metal, if they are able to penetrate the Ni barrier layer. The average distance for diffusion of filler metal elements in Ni is 7.0 and 4.8 μm for Ag 155 and ZnGaCu-(AuSn), respectively, significantly less for ZnGaCu-(AuSn) than Ag 155. A typical Ni diffusion barrier layer can be 10 μm or more in thickness, so the recorded diffusion distances seem suitable (though it does of course neglect any diffusion occurring over extended times in service conditions) in the nickel parent material.

The electrical contact resistance depends on the specific type of materials used. It should be as low as possible to minimise the impact of resistive effects on the energy conversion efficiency. However, in brazing it is possible that interphases could form at the joint; these would lead to an increase of contact resistance [45–47], and it is therefore important to avoid or reduce their formation if possible. Solid solutions are considered to be more likely to form in HEA alloys and therefore, intermetallics could be restrained reducing the contact resistance at the interface. Fig. 10 and Table 6 show that the resistance discontinuity of the interfaces is 0.92 and 1.07 mΩ, respectively. The average electrical contact resistance of these two interfaces is 11.2×10^{-5} Ωcm^{-2}. In similar joins, such as between copper and a $CoSb_3$ material [48], the maximum contact resistance requirement is 5×10^{-5} Ωcm^{-2}. In other investigations of filler metals, for joints consisting of n-type half-Heusler ($Ti_{0.6}Hf_{0.4}NiSn$)/(Incusil filler)/Ag/(Incusil filler)/half-Heusler, the contact resistance of the half-Heusler/Incusil interface was found to decrease from 100×10^{-5} Ωcm^{-2} at room temperature to 5×10^{-5} Ωcm^{-2} at 500 C [13] (although it should be noted there are examples of studies with better contacts where the impact of temperature is less dramatic [49]). The average electrical contact resistance in this study is, as measured, slightly more than double the target value for a similar system, but it is lower than that in the n-type half-Heusler joints at room temperature. Therefore, the performance of the designed HEA filler is promising, and overall, this new HEA ZnGaCu-(AuSn) alloy has great potential as a filler metal. Further characterisation (such as of mechanical strength, which has not been explored here as the joints are not expected to bear any structural load beyond the weight of the thermoelectric) would be valuable, as would the exploration of the performance with a wider range of thermoelectric materials. The methodology used here is effective to design new filler metals, and potentially other alloys, through large scale computational screening.

6. Conclusions

Five High Entropy Alloys (HEAs), ZnGaCu-(Al), ZnGaCu-(Ni), ZnGaCu-(NiGe), ZnGaCu-(AuSn) and ZnGaCu-(AuBi), were selected as filler metal candidates for brazing nickel to copper after selection calculations carried out via Python programming. The ZnGaCu-(AuSn) alloy (atomic ratio of 36:26: 30: 6: 2) has shown the best brazeability with good joining behaviour and macro- and micro-scale appearance, as compared with other filler candidates.

A solid solution (designated here as SS-Au-1), Sn, $CuGa_2$ and Au–Ga phases were found in ZnGaCu-(AuSn). This new alloy demonstrated the potential to wet and join copper and nickel with a melting temperature range of 529–674 °C., and a final liquid contact angle on a copper substrate of 47.0 ± 1.8° over the range 765 °C to 800 °C. The diffusion distance of elements from the ZnGaCu-(AuSn) alloy in Ni is 4.8 μm, which is suitable to avoid interaction with the skutterudite thermoelectric component during processing.

A promising average contact interface resistance of 11.2×10^{-5}Ωcm^{-2} was obtained at room temperature when used to join skutterudite thermoelectrics ($CoSb_{2.75}Sn_{0.05}Te_{0.20}$ with Ni coating). Therefore, this new HEA alloy has great potential as a filler metal in such applications.

CRediT authorship contribution statement

Matthew Way: Investigation, Data curation, Formal analysis, Writing - original draft. **Dan Luo:** Formal analysis, Visualization, Writing - review & editing. **Richard Tuley:** Investigation, Resources, Writing - review & editing. **Russell Goodall:** Formal analysis, Supervision, Writing - review & editing.

Declaration of competing interest

The authors declare that they have no known competing financial interests or personal relationships that could have appeared to influence the work reported in this paper.

Acknowledgment

MW would like to thank Johnson Matthey plc and the EPSRC for the provision of an ICASE PhD studentship. DL and RG would like to acknowledge funding from the EPSRC (grant number EP/S032169/1).

Appendix A. Supplementary data

Supplementary data to this article can be found online at https://doi.org/10.1016/j.jallcom.2020.157750.

References

[1] T. Phongpreecha, J.D. Nicholas, T.R. Bieler, Y. Qi, Computational design of metal oxides to enhance the wetting and adhesion of silver-based brazes on yttria-stabilized-zirconia, Acta Mater. 152 (2018) 229–238.
[2] C. Xin, J. Yan, Q. Wang, W. Feng, C. Xin, The microstructural evolution and formation mechanism in Si3N4/AgCuTi/Kovar braze joints, J. Alloys Compd. 820 (2020) 153189.
[3] Z. Sun, Y.K. Ma, B. Zhang, L.X. Zhang, Controlling interfacial reactions of Ti_3SiC_2/Ti_2AlNb brazed joints by transferring graphene layers, Mater. Sci. Eng., A 771 (2020) 138624.
[4] M.J. Benoit, H. Jin, B. Shalchi-Amirkhiz, S. Kurukuri, S. Winkler, M.J. Worswick, M.A. Wells, Microstructure evolution of warm deformed multilayered Al alloy sheet during brazing, J. Mater. Process. Technol. 281 (2020) 116639.
[5] J. de Prado, M. Sánchez, G. Stan, A. Galatanu, A. Ureña, Effect of Cr and V coatings on W base material in W-Eurofer brazed joints for fusion applications, Fusion Eng. Des. 159 (2020) 111748.
[6] Y. Zhou, A. Hu, From microjoining to nanojoining, Open Surf. Sci. J. 3 (2010) 32–41.
[7] W. Wu, A. Hu, X. Li, J.Q. Wei, Q. Shu, K.L. Wang, M. Yavuz, Y.N. Zhou, Vacuum brazing of carbon nanotube bundles, Mater. Lett. 62 (2008) 4486–4488.
[8] M. Way, J. Willingham, R. Goodall, Brazing filler metals, Int. Mater. Rev. (2019) 1–29, 0.
[9] D. Champier, Thermoelectric generators: a review of applications, Energy Convers. Manag. 140 (2017) 167–181.
[10] R. He, G. Schierning, K. Nielsch, Thermoelectric devices: a review of devices, architectures, and contact optimization, Adv. Mater. Technol. 3 (2018) 1700256.
[11] H.Y. Xia, C.L. Chen, F. Drymiotis, A. Wu, Y.Y. Chen, G.J. Snyder, Interfacial reaction between Nb foil and n-type PbTe thermoelectric materials during thermoelectric contact fabrication, J. Electron. Mater. 43 (11) (2014) 4064–4069.
[12] Z.G. Shen, L.L. Tian, X. Liu, Automotive exhaust thermoelectric generators: current status, challenges and future prospects, Energy Convers. Manag. 195 (2019) 1138–1173.
[13] P.H. Ngan, N.V. Nong, L.T. Hung, B. Balke, L. Han, E.M.J. Hedegaard, S. Linderoth, N. Pryds, On the challenges of reducing contact resistances in

thermoelectric generators based on half-Heusler alloys, J. Electron. Mater. 45 (2016) 594–601.
[14] L.F. Shi, X.Y. Huang, M. Gu, L.D. Chen, Interfacial structure and stability in Ni/SKD/Ti/Ni skutterudite thermoelements, Surf. Coating. Technol. 285 (2016) 312–317.
[15] S.W. Chen, A.H. Chu, D.S.H. Wong, Interfacial reactions at the joints of CoSb3-based thermoelectric devices, J. Alloys Compd. 699 (2017) 448–454.
[16] F. Wu, Q. He, D. Hu, F. Gao, H. Song, J. Jia, X. Hu. Thermal decomposition of thermoelectric material CoSb3: a thermogravimetry kinetic analysis. J. Electron. Mater. 42(8): 2574–2581.
[17] Iso/Tc 44, Brazing — Filler Metals, third ed., British Standards Institution, 2016 (ISO 17672:2016).
[18] BSI BSI. BS EN ISO 9453, BSI Standards Publication Soft Solder Alloys — Chemical Compositions and Forms. 2014, 2014.
[19] European Commission, Commission Regulation (EU) No 494/2011 vols. 2–5, Off. J. Eur. Union, 2011.
[20] H. Okamoto, Ag-Sb (Silver-Antimony), J. Phase Equilibria Diffus. 28 (4) (2007) 403.
[21] H. Feng, L. Zhang, J. Zhang, W. Gou, S. Zhong, G. Zhang, H. Geng, J. Feng, Metallization and Diusion Bonding of CoSb3-Based Thermoelectric Materials vol. 13, 2020, p. 1130.
[22] M. Braunovid, N. Aleksandrov, Intermetallic compounds at aluminum-to-copper and copper-to-tin electrical interfaces, Electr. Contacts, Proc. Annu. Holm Conf. Electr. Contacts. October (1992) 25–34.
[23] J. Zhang, J. Gu, L. Li, Y. Huan, B. Wei, Bonding of alumina and metal using bulk metallic glass forming alloy, Int. J. Mod. Phys. B 23 (2009) 1306–1312.
[24] R. Sun, Y. Zhu, W. Guo, P. Peng, L. Li, Y. Zhang, J. Fu, Microstructural evolution and thermal stress relaxation of Al2O3/1Cr18Ni9Ti brazed joints with nickel foam, Vacuum 148 (2018) 18–26.
[25] L.X. Zhang, J.M. Shi, H.W. Li, X.Y. Tian, J.C. Feng, Interfacial microstructure and mechanical properties of ZrB2-SiC-C ceramic and GH99 superalloy joints brazed with a Ti-modified FeCoNiCrCu high-entropy alloy, Mater. Des. 97 (2016) 230–238.
[26] W. Tillmann, T. Ulitzka, L. Wojarski, M. Manka, H. Ulitzka, D. Wagstyl, Development of high entropy alloys for brazing applications, Weld. World 64 (2020) 201–208.
[27] R. Snell, The development of novel silver brazing alloys, PhD Thesis, 2017.
[28] Q. Ding, Y. Zhang, X. Chen, X. Fu, D. Chen, S. Chen, et al., Tuning element distribution, structure and properties by composition in high-entropy alloys, Nature 574 (2019) 223–227.
[29] B. Yin, F. Maresca, W.A. Curtin, Vanadium is an optimal element for strengthening in both fcc and bcc high-entropy alloys, Acta Mater. 188 (2020) 486–491.
[30] D.B. Miracle, O.N. Senkov, A critical review of high entropy alloys and related concepts, Acta Mater. 122 (2017) 448–511.
[31] J.W. Yeh, Alloy design strategies and future trends in high-entropy alloys, J. Occup. Med. 65 (2013) 1759–1771.
[32] D. Bridges, S. Zhang, S. Lang, M. Gao, Z. Yu, Z. Feng, A. Hu, Laser brazing of a nickel-based superalloy using a Ni-Mn-Fe-Co-Cu high entropy alloy filler metal, Mater. Lett. 215 (2018) 11–14.
[33] W. Tilllmann, T. Ulitzka, L. Wojarski, et al., Brazing of high temperature materials using melting range optimized filler metals based on the high-entropy alloy CoCrCuFeNi, Brazing, High Temp. Brazing Diffus. Bond. LÖT (2019).
[34] L. Hardwick, P. Rodgers, E.J. Pickering, et al., Development of novel nickel-based brazing alloys, utilising alternative melting point depressants and high entropy alloy concepts, Brazing, High Temp. Brazing Diffus. Bond. LÖT (2019).
[35] G. Wang, Y. Yang, R. He, G. Tan, M. Huttula, W. Gao, A novel high entropy CoFeCrNiCu alloy filler to braze SiC ceramics, J. Eur. Ceram. Soc. 40 (2020) 3391–3398.
[36] L. Pu, Q. He, Y. Yang, X. Zhao, Z. Hou, K.N. Tu, Y. Liu, The microstructure and mechanical property of the high entropy alloy as a low temperature solder, in: IEEE 69th Electronic Components and Technology Conference, ECTC), 2019.
[37] Y. Zhang, Y.J. Zhou, J.P. Lin, G.L. Chen, P.L. Liaw, Solid-solution phase formation rules for multi-component alloys, Adv. Eng. Mater. 10 (2008) 534–538.
[38] L. Gremilard, N. Rauch N, E. Saiz, Drop Angle, Lawrence Berkeley National Laboratory, Berkeley, 2002.
[39] W. Liu, H. Wang, L. Wang, X. Wang, G. Joshi, G. Chen, Z. Ren, Understanding of the contact of nanostructured thermoelectric n-type $Bi_2Te_{2.7}Se_{0.3}$ legs for power generation applications, J. Mater. Chem. A 1 (2013) 13093–13100.
[40] Z. Yang, J. PradoGonjal, M. Phillips, S. Lan, A. Powell, P. Vaqueiro, M. Gao, R. Stobart, R. Chen, Improved Thermoelectric Generator Performance Using High Temperature Thermoelectric Materials, SAE Technical Paper, 2017, 2017-01-0121.
[41] S. Murarka, M. Anand, R. Agarwala, Diffusion of vanadium in aluminium and nickel, Acta Metall. 16 (1) (1968) 69–72.
[42] A.R. Wazzan, P. Tung, L.B. Robinson, Diffusion of silver into nickel single crystals, J. Appl. Phys. 42 (13) (1971) 5316–5320.
[43] S. Mantl, S. Rothman, L. Nowicki, J. Lerner, The tracer diffusion of Ge in Ni single crystals, J. Phys. F Met. Phys. 13 (7) (1983) 1441–1448.
[44] P. Neuhaus, C. Herzig, W. Gust, Grain boundary diffusion of indium in nickel and nickel-indium, Acta Metall. 37 (2) (1989) 587–595.
[45] S.M. Choi, K.H. Kim, S.M. Jeong, H.S. Choi, Y.S. Lim, W.S. Seo, I.H. Kim, A resistance ratio analysis for $CoSb_3$-based thermoelectric unicouples, J. Electron. Mater. 41 (6) (2012) 1004–1010.
[46] P. Sun, C. Andersson, X. Wei, Z. Cheng, D. Shangguan, J. Liu, High temperature aging study of intermetallic compound formation of Sn–3.5Ag and Sn–4.0Ag–0.5Cu solders on electroless Ni(P) metallization, J. Alloys Compd. 425 (2006) 191–199.
[47] Y. Thimont, Q. Lognone, C. Goupil, F. Gascoin, E. Guilmeau, Design of apparatus for Ni/Mg_2Si and Ni/MnSi1.75 contact resistance determination for thermoelectric legs, J. Electron. Mater. 43 (6) (2014) 2023–2028.
[48] K.T. Wojciechowski, R. Zybala, R. Mania, High temperature $CoSb_3$–Cu junctions, Microelectron. Rellab. 51 (2011) 1198–1202.
[49] J. de Boor, C. Gloanec, H. Kolb, R. Sottong, P. Ziolkowski, E. Müller, Fabrication and characterization of nickel contacts for magnesium silicide based thermoelectric generators, J. Alloys Compd. 632 (2015) 348–353.